

Photon Counting with Silicon Avalanche Photodiodes

Xiaoli Sun, *Member, IEEE*, and Frederic M. Davidson, *Senior Member, IEEE*

Abstract—Avalanche photodiodes (APD's) are studied for use as photon counting detectors. The APD may be biased slightly above (Geiger mode) or slightly below its voltage breakdown point. In the latter case, if the photon absorption rate is low enough, each individual photoelectron current pulse may be resolved with the use of a discriminator. APD's used in this photon counting mode are shown to give the best performance at low light levels. Experimentally, overall photon detection probabilities of 5.0 and 0.33% were obtained at $\lambda=820$ nm and $\lambda=1.064$ μm , respectively, with a photon counter dead time as low as 15 ns and a dark current counting rate of 7000/s. The APD photon counter exhibited an exponential photon interarrival time probability density and a near Poissonian photon counting probability.

I. INTRODUCTION

AlGaAs laser diodes and diode laser pumped Nd:YAG lasers are among the most attractive laser sources for industry and scientific research because of their small size, high electrical to optical conversion efficiency, high output power, and long lifetime. In many applications, photon counting is required in order to achieve the highest, or quantum limited, detector performance. The quantum efficiencies of conventional photomultiplier tubes (PMT) start to decrease rapidly at the wavelengths of AlGaAs laser diodes ($\lambda \sim 800$ nm) and drop to about 0.1% at the fundamental wavelength of Nd:YAG lasers ($\lambda = 1.064$ μm) [1]. Silicon avalanche photodiodes (APD) have relatively high quantum efficiencies which are 70–90% at $\lambda = 800$ nm [2], and typically 6% but can be as high as 40% at $\lambda = 1.064$ μm [3]. This paper investigates the use of APD's as individual photon counting photodetectors, and reports the results of photon counting experiments carried out with a silicon APD biased below its breakdown voltage.

APD's are normally operated in either analog or avalanche breakdown photon counting (Geiger) modes. In analog mode, an APD is biased slightly below the breakdown voltage such that the average output current is proportional to the incident optical power and equal to the primary photocurrent multiplied by an average internal avalanche gain. In the avalanche breakdown photon counting mode, an APD is biased above the breakdown voltage such that individual detected photons trigger an avalanche breakdown which results in a strong output current spike that can then be individually counted [4]. The performance of APD's in analog mode are limited by the amplifier thermal noise and the APD excess noise due to the randomness of the APD gain mechanism. On the other

hand, APD's in avalanche breakdown photon counting mode are subject to afterpulsing and a relatively long dead time due to the slow recovery process after each avalanche breakdown.

When the received light level is low enough, individual photoelectron current pulses may be resolved in the output photocurrent with the APD biased slightly below the breakdown voltage. Each photon absorption will result in a photocurrent pulse but the amplitude of the pulse is much smaller than that output by an APD biased above the breakdown point. Consequently, a high gain low noise amplifier and discriminator are required to detect these relatively weak photocurrent pulses. The APD should be biased such that the highest stable value of average gain is achieved. The dead time of this type of photon counter is limited only by the gain-bandwidth product of the APD and the bandwidth of the subsequent circuits. The major obstacle toward implementation of this type of APD photon counter has been the lack of wide band and low noise APD preamplifiers. Kikuchi *et al.* (1985) first implemented and tested such a nonbreakdown APD photon counter, in which the APD and preamplifier were held at 77°K in order to reduce thermal noise [5]. Lightstone and McIntyre (1988) gave a partial characterization of this type of APD photon counter along with some measurement data at room temperature [6]. However, the dead time of their experimental photon counter was rather long (> 0.5 μs) because the electrical bandwidth had to be kept relatively small in order to find a preamplifier with sufficiently low thermal noise.

We have developed a complete theoretical model to characterize this type of nonbreakdown APD photon counter. Preliminary experimental results were shown to agree with the theoretically predicted values. The measured photon counts appeared to have a Poisson distribution and the interarrival times fit an exponential distribution, as expected. The dead time was measured to be about 15 ns, which is the shortest yet reported for APD photon counters operated in either nonbreakdown or breakdown mode. The overall photon detection probability was about 5.0% at $\lambda = 820$ nm and about 0.33% at $\lambda = 1.064$ μm . It is predicted that the overall photon detection efficiency can be improved to as high as 20% at $\lambda = 820$ nm and 1.5% at $\lambda = 1.064$ μm with a dead time of a few nanoseconds by using a state-of-the-art silicon APD and a more advanced commercially available transimpedance preamplifier. Such photon counters will have wide applications in photo-electric sensing instruments, optical communications, lidars, laser altimeters, and light scattering spectroscopies.

The rest of this paper is organized as follows. Section II gives a brief review of APD's in avalanche breakdown photon counting mode. Section III gives a detailed description and

Manuscript received May 14, 1991; revised March 16, 1992. This work is supported by NASA Goddard Space Flight Center.

The authors are with the Department of Electrical and Computer Engineering, The Johns Hopkins University, Baltimore, MD 21218.

IEEE Log Number 9200838.

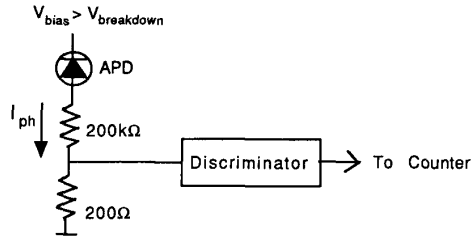


Fig. 1. Typical circuit diagram of an avalanche breakdown type APD photon counter according to [2].

performance analysis of APD photon counters under non-breakdown operation. The experiments and measurement data are presented in Section IV. Section V contains conclusions along with some predictions of performance of APD's in nonbreakdown photon counting mode when used with more advanced electro-optical and electronic devices.

II. REVIEW OF APD'S UNDER AVALANCHE BREAKDOWN PHOTON COUNTING OPERATION

An APD can be biased several volts above its breakdown point for photon counting operation [2], [4]. Avalanche breakdowns are triggered by both absorbed photons and thermally generated hole-electron pairs inside the device. Each avalanche breakdown results in a large current spike which can be easily detected by a discriminator. Fig. 1 shows a diagram of a typical APD breakdown photon counting circuit [2].

Since not all the received photons can trigger avalanche breakdowns, the average number of photons counted by the discriminator, \bar{n}_c , is always less than the average number of absorbed photons, \bar{n} . The overall photon detection probability, P_d , can be written as

$$P_d = \eta_Q \frac{\bar{n}_c}{\bar{n}} = \eta_Q P_{trig} \quad (1)$$

where η_Q is the quantum efficiency of the APD, P_{trig} is the probability that an absorbed photon triggers an avalanche breakdown which results in a discriminator threshold crossing. The average number of absorbed photons, \bar{n} , over a counting interval, T , is related to the received optical power, P_o , by

$$\bar{n} = \frac{\eta_Q P_o T}{hf} \quad (2)$$

where hf is the photon energy. The number of photons being counted, n , should be a Poisson random variable with mean equal to \bar{n}_c . A signal to noise ratio (SNR) may be defined as the ratio of the mean to the standard deviation of the number of detected photons. Considering the background noise counts and dark counts, the SNR of the detected number of photons is given by

$$SNR = \frac{P_{trig} \bar{n}_s}{[P_{trig}(\bar{n}_s + \bar{n}_{bg}) + \bar{n}_{dark}]^{1/2}} \quad (3)$$

where \bar{n}_s and \bar{n}_{bg} are the average numbers of absorbed signal and background photons, and \bar{n}_{dark} is the average number of total dark counts caused by the APD dark current and circuit thermal noise.

The probability of triggering, P_{trig} , increases with the bias voltage and so does the dark count rate. The value of P_{trig} is typically 7% with 15 000/s dark counts at 22°C when the APD is biased approximately two volts above the breakdown point [2]. Although higher values of P_{trig} (50–80%) can be achieved at even higher bias voltages [4], they cannot be used in most applications because of the excessively high dark count rates and other nonlinear effects. The dark counts can be reduced by cooling the APD. However, the quantum efficiency of the APD may also decrease with temperature over certain wavelength ranges. For example, for a RCA-C30902S silicon APD, the dark count rate decreases from 15 000/s at 20°C to 300/s at –25°C, but the quantum efficiency also decreases by about a factor of two at $\lambda = 1.064 \mu\text{m}$ [2].

A major disadvantage of breakdown type APD photon counters is the existence of so called “afterpulsing” due to excess avalanche breakdowns which appear randomly after each avalanche breakdown. The cause of afterpulsing is attributed to the presence of charges trapped at dislocations and impurities in the high voltage region of the APD after each avalanche breakdown [6]. At room temperature, afterpulsing occurs randomly at 10^{-9} to 10^3 s after each avalanche breakdown but they are mainly distributed within the first few microseconds [2], [4]. The probability of afterpulsing from 1 ms to 60 s is typically 2–15% [2] and increases with the APD bias voltage. Afterpulsing is a nonlinear effect and has not been well understood except for some simplified mathematical modeling [7]. Afterpulses appear as a source of correlated and signal dependent random noise, which can be overwhelming in many sensitive measurements.

The dead time of a breakdown APD photon counter is mainly determined by the recovery process of the APD after each avalanche breakdown. Every time a breakdown occurs, the APD current has to be quenched to prevent “latching” into a continuous discharge state. There are two types of quenching circuits: passive quenching and active quenching. One example of passive quenching is shown in Fig. 1. When a breakdown occurs, the voltage drop across the resistors in series with the APD effectively reduces the APD bias voltage to below the breakdown point. The APD bias voltage is then gradually restored as the APD shunt capacitance gets recharged. Since the resistors have to be relatively large to limit the maximum APD current, the recovery process is relatively slow. The typical dead time of this type of photon counter is about one microsecond [2], [8]. An active quenching circuit can significantly shorten the dead time by momentarily reducing the resistance in series with the APD after each breakdown has been quenched, so that the APD shunt capacitance can be charged with a much shorter time constant than that of a passive quenching circuit. Brown *et al.* [9] have reported an active quenching circuit which achieved a dead time of a few tens of nanoseconds.

Because of the existence of a finite dead time, photons which arrive within the dead time cannot be resolved and the number of detected photons is no longer a Poisson random variable. Cantor and Teich [10] have shown that the probability that n' photons are counted over a T second interval in response to \bar{n} average absorbed photons for a given dead time, τ_d , can

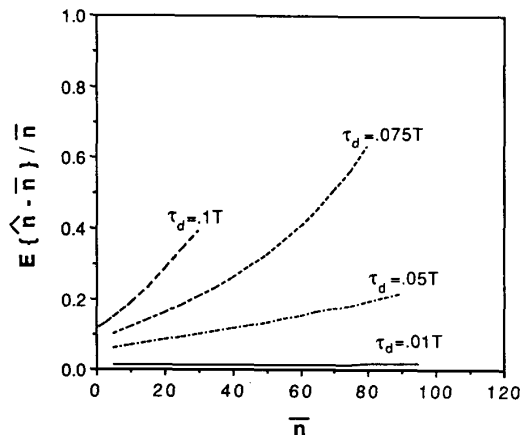


Fig. 2. Normalized average estimation error, $E\{\hat{n} - \bar{n}\}/\bar{n}$, of the ML estimator as a function of the average number of absorbed photons, \bar{n} for a given dead time, τ_d , and a counting interval, T .

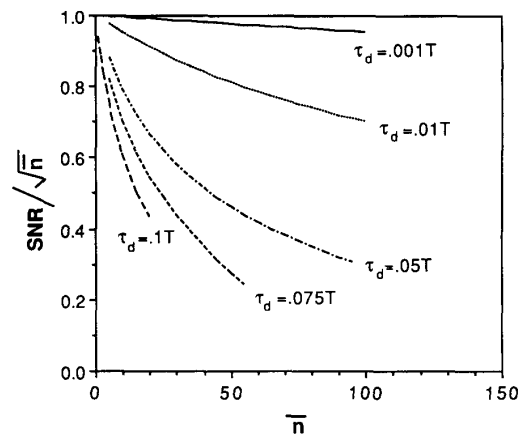


Fig. 3. Normalized SNR of the ML estimator as a function of the average number of absorbed photons, \bar{n} , for a given dead time, τ_d , and a counting interval, T .

be written as

$$\Pr(n' | \bar{n}, \tau_d) = \sum_{k=0}^{n'} \frac{[\bar{n}(1 - \frac{\tau_d}{T}n')]^k}{k!} e^{-\bar{n}(1 - \frac{\tau_d}{T}n')} - \sum_{k=0}^{n'-1} \frac{\{\bar{n}[1 - (n'-1)\frac{\tau_d}{T}]\}^k}{k!} e^{-\bar{n}[1 - (n'-1)\frac{\tau_d}{T}]}, n' < \frac{T}{\tau_d}. \quad (4)$$

The maximum likelihood (ML) estimator, \hat{n} , of the average number of actually absorbed photons, \bar{n} , given n' detected photons under this condition is given by [11]

$$\hat{n} = \frac{n'}{1 - n'(\tau_d/T)}. \quad (5)$$

When the dead time is zero, i.e., $\tau_d = 0$, (4) reduces to a Poisson distribution and (5) reduces to $\hat{n} = n' = n$ which is the actual number of photons counted. The mean of the ML estimator is the same as the average number of absorbed photons, \bar{n} , and the SNR under this condition is equal to $\bar{n}^{1/2}$.

When the dead time is not zero, the ML estimator given by (5) always results in a nonzero average estimation error and a larger standard deviation, i.e., $|E\{\hat{n}\} - \bar{n}| = \epsilon > 0$ and $\sigma\{\hat{n}\} > \bar{n}^{1/2}$. As a result, the signal to noise ratio is always smaller than that when the dead time is zero, i.e., $SNR_{\hat{n}} < \bar{n}^{1/2}$. Figs. 2 and 3 show the normalized average estimation error and SNR as a function of average number of absorbed photons.

III. APD'S UNDER NONBREAKDOWN PHOTON COUNTING OPERATION

APD's may be used to count single photons while biased below the breakdown point as in analog mode [5], [6]. The photocurrent pulses resulting from a single photon absorption can be detected via a discriminator threshold crossing with a relatively high probability as long as the APD gain is sufficiently large and the circuit thermal noise is relatively

low. There is effectively no afterpulsing since the APD is operating in its linear regime at much lower gains than in breakdown mode. The dead time can also be much shorter than that of a breakdown type APD photon counter since the APD bias voltage does not need to be restored after each photon detection. The receiver could be operated in both photon counting and analog modes simultaneously by diverting part of the APD preamplifier output to an analog channel. The analog channel can operate linearly after the photon counting channel is saturated due to a strong input light intensity. Therefore, the dynamic range of the entire receiver can be greatly extended.

A. Principle of Operation

The circuit used for this type of photon counter is shown in Fig. 4. The APD and preamplifier are exactly the same as those in the analog mode except that the average APD gain is set to the highest achievable value but not necessarily the value which optimizes SNR of the output. This requires a very stable bias voltage supply and may need some form of APD temperature control or compensation. The output of the preamplifier is compared against a threshold with the use of a comparator or a discriminator whose output is connected to an electrical pulse counter. The threshold level of the discriminator has to be carefully set in order to achieve a high photon detection probability while maintaining an acceptable noise count rate. The dead time of this type of photon counter is limited by the photocurrent pulse width which is about equal to the reciprocal of the bandwidth of the APD and preamplifier. The bandwidth of the APD is limited by its maximum gain-bandwidth product. In practice, the dead time is longer than the pulse width because of the limited time resolution of the discriminator and the electrical pulse counter. Since the APD gain is random, the pulse width is a random variable and so is the dead time. The actual dead time distribution usually has to be determined experimentally.

The number of detected signal photon counts and the number of dark counts are both Poisson random variables. The signal to noise ratio can be computed using (3) by substituting

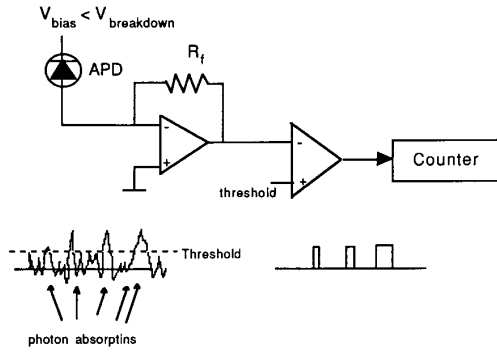


Fig. 4. Circuit diagram of a nonbreakdown type APD photon counter.

the threshold crossing (discrimination) probability, P_{disc} , for the triggering probability, P_{trig} .

B. Effective Quantum Efficiency

Since the APD gain is random, not all the photon absorptions result in photocurrent pulses whose peak amplitudes are large enough to cross the discriminator threshold. The photon detection probability can be written, similarly to (1), as

$$P_d = \eta_Q \times \frac{E\{\text{photons counted}\}}{E\{\text{photons absorbed}\}} = \eta_Q P_{disc} \quad (6)$$

where P_{disc} is the probability that a photocurrent pulse in response to a photon absorption is discriminated against the noise floor. The computation of P_{disc} is given as follows.

Ideally, the photocurrent pulse output from an APD in response to a photon absorption should be an impulse and the preamplifier consists of equivalently a resistor and a capacitor in parallel. The pulse shape output from the preamplifier is an exponential function and the average area under the pulse shape function is mq with m the instantaneous APD gain and q the electron charge. The peak amplitude of the pulse is given by $i_{phmax} = mq/RC = 2\pi mqB_{3dB}$ with $B_{3dB} = 1/2\pi RC$, the 3-dB bandwidth of the preamplifier. In practice, the APD output cannot be true impulses and the frequency response of the preamplifier is not exactly the same as that of a RC filter. As a result, the shapes of the actual photocurrent pulses output from the APD preamplifier are not true exponential functions but have a finite rise time, a round peak, and a slower trailing edge. Empirically, we choose

$$i_{phmax} = 4mqB_{3dB}, \quad (7)$$

which seems to yield results consistent with the measurements.

A photon is detected whenever the peak amplitude of a photocurrent pulse exceeds the threshold current, I_{thr} . The value of i_{phmax} is a discrete random variable. The probability of discrimination, P_{disc} , is given by

$$\begin{aligned} P_{disc} &= \text{Prob}(i_{phmax} > I_{thr}) = \text{Prob}(m \geq M_{thr}) \\ &= 1 - \sum_{m=1}^{M_{thr}-1} \text{Pr}(m) \end{aligned} \quad (8)$$

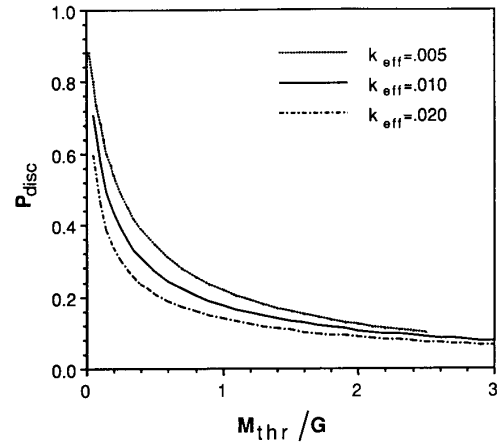


Fig. 5. Probability of discrimination, P_{disc} , of a nonbreakdown APD photon counter versus the equivalent threshold gain, M_{thr} .

where M_{thr} is the equivalent threshold crossing APD gain given by

$$M_{thr} = \frac{I_{thr}}{4qB_{3dB}} \quad (9)$$

and $\text{Pr}(m)$ is the the probability distribution of the APD gain. McIntyre and Conradi [12], [13] have shown that the probability of the APD gain can be written as

$$\begin{aligned} \text{Pr}(m) &= \frac{\Gamma\left(\frac{m}{1-k_{eff}} + 1\right)}{m! \Gamma\left(\frac{k_{eff}m}{1-k_{eff}} + 2\right)} \cdot \left[\frac{1 + k_{eff}(G-1)}{G} \right]^{\frac{k_{eff}m}{1-k_{eff}} + 1} \\ &\cdot \left[\frac{(1-k_{eff})(G-1)}{G} \right]^{m-1} \end{aligned} \quad (10)$$

with $\Gamma(\cdot)$ the Gamma function. The photon detection probability of this type of photon counter can be evaluated by substituting (9) and (10) into the right-hand side of (8) and then (6). Fig. 5 plots P_{disc} as a function of the equivalent threshold crossing APD gain normalized with respect to the average APD gain, G , for $G=1000$ and the APD ionization coefficient ratios $k_{eff} = 0.005, 0.010$, and 0.020 , respectively. It is seen that the smaller the k_{eff} , the larger the P_{disc} .

C. Dark Counts

There are two sources of dark counts: the APD dark current and the circuit thermal noise. The APD dark current consists of surface leakage current and bulk leakage current. The former does not pass through the high gain region of the APD and hardly causes any dark counts. The latter does pass through the high gain region of the APD and acts as a source of background radiation. The number of dark counts due to a bulk leakage current, I_b , can be modeled as a Poisson random variable with the mean equal to

$$\bar{n}_{dark1} = P'_{disc} \frac{I_b T}{q} \quad (11)$$

where P'_{disc} is the average probability that an electron of the APD bulk leakage current causes a discriminator threshold

crossing. The value of P'_{disc} should be smaller than that for a primary photoelectron, since part of the APD bulk leakage current is generated inside the APD high field region and is not multiplied by the full APD gain. We have found experimentally that $P'_{disc} \approx 0.17P_{disc}$ for a RCA-C30902S silicon APD which had a bulk leakage current of $I_b \approx 0.1$ pA.

The number of dark counts due to circuit thermal noise should also follow a Poisson distribution if the correlation time of the noise is less than the dead time of the photon counter. The average number of counts due to circuit noise, \bar{n}_{dark2} , over a counting interval of T seconds can be written as [14]

$$\bar{n}_{dark2} = (T/\bar{\Delta}t)P_{fa} \quad (12)$$

where $\bar{\Delta}t$ is the average threshold crossing time or pulse width which is about equal to the reciprocal of the bandwidth, and P_{fa} is the threshold crossing probability due to the circuit thermal noise at a fixed sampling time.

The equivalent circuit noise current at the input of the preamplifier can be modeled as a zero mean Gaussian random process. The preamplifier usually contains an FET as the input stage. The variance of the equivalent noise current at any time t is given approximately by [15], as

$$\sigma_{amp}^2 = \frac{1}{2\pi} \int_0^\infty \left[\frac{4KT_a}{R_f} + 2qI_g + \frac{4KT_a\gamma}{g_m R_f^2} + \frac{4KT_a\gamma(\omega C_i)^2}{g_m} \right] \left| \frac{Z(\omega)}{R_f} \right|^2 d\omega \quad (13)$$

where K is Boltzmann's constant, T_a is the FET temperature in Kelvin, R_f is the feedback resistance, I_g is the FET gate leakage current, g_m is the transconductance of the FET, γ is a numerical factor close to unity, C_i is the total input capacitance, and $Z(\omega)$ is the transfer function of the transimpedance amplifier. For most commercial high-speed transimpedance preamplifiers, the integrand in (13) can be assumed to be constant over its useful bandwidth. Under this condition, an equivalent noise temperature, T_e ($^\circ\text{K}$) can be defined such that the total amplifier noise is equal to the thermal noise generated by the feedback resistor at temperature T_e . The total amplifier noise can then be written approximately as

$$\sigma_{amp}^2 = \frac{4KT_e}{R_f} B_n \quad (14)$$

where B_n is the noise bandwidth given by

$$B_n = \frac{1}{2\pi} \int_0^\infty \left| \frac{Z(\omega)}{R_f} \right|^2 d\omega \quad (15)$$

If the transimpedance preamplifier can be modeled as a RC filter, the noise bandwidth is 1.57 times the 3-dB bandwidth [16]. The threshold crossing probability can be expressed as

$$P_{fa} = \int_{I_{thr}}^\infty \frac{1}{\sqrt{2\pi\sigma_{amp}^2}} e^{-\frac{u^2}{2\sigma_{amp}^2}} du \quad (16)$$

There is always a trade-off between the photon detection probability and circuit noise counts. Both P_{disc} and \bar{n}_{dark2} decrease as the threshold I_{thr} increases. For best performance,

the threshold level should be set such that the total number of dark counts is much less than that of the photon counts, i.e., $\bar{n}_{dark1} + \bar{n}_{dark2} \ll \bar{n}P_{disc}$. If the value of the average number of absorbed photons, \bar{n} , is completely unknown and needs to be determined through the measurement, the threshold level should be set such that the dark counts due to circuit noise are much less than those due to the APD bulk leakage current, i.e., $\bar{n}_{dark2} \ll \bar{n}_{dark1}$. Usually, the threshold is set to be a few times the standard deviation of the circuit noise, i.e., $I_{thr} = f \times \sigma_{amp}$ with f a multiplication factor. The equivalent threshold crossing gain in (9) can be expressed as

$$M_{thr} = 0.626f \sqrt{\frac{KT_e}{R_f B_{3dB}}} \quad (17)$$

The probability of discrimination and the photon detection probability can be evaluated by substituting (17) and (10) into (8) and (6). If the photon counter is operating properly, the numbers of detected signal and background photons, the dark counts due to APD leakage current, and the dark counts due to circuit thermal noise should all follow Poisson distributions, and so should the total number of counts.

As seen in (17), the equivalent APD threshold crossing gain M_{thr} is inversely proportional to the square root of the feedback resistance R_f and the 3-dB bandwidth of the preamplifier. Since the probability of discrimination, P_{disc} , increases as M_{thr} decreases, it is important to keep the product of the feedback resistance and the 3-dB bandwidth of the transimpedance preamplifier as large as possible in order to achieve a high photon detection probability.

IV. EXPERIMENTS WITH NONBREAKDOWN APD PHOTON COUNTERS

An experimental nonbreakdown APD photon counter was built and the performance was measured to verify the theoretical model developed in the previous section.

A. Experimental Setup

Fig. 6 shows the optical setup of the experiment. The light source consisted of a low voltage incandescent light bulb, a diffuser, a pinhole, and a collimating lens. The light bulb was powered by a stable dc voltage supply. The light beam was first attenuated and then filtered through two interference filters which were centered at $\lambda = 821$ nm and had a combined bandwidth of $\Delta\lambda = 7$ nm. The light after the interference filter can be considered to have an almost perfectly constant intensity and the counting statistics of the photons can be shown to follow a Poisson distribution [17]. The received optical power was measured directly by substituting an optical power meter sensor head for the APD which could be moved aside. The experiment was conducted at room temperature and in total darkness. A universal counter (Stanford Research Systems SR620) was used to count the pulses output from the discriminator.

The details of the electronics are shown in Fig. 7. The APD used was a RCA-C30902S silicon APD with $k_{eff} = 0.010$, $I_b \approx 0.1$ pA, and $I_s = 12$ nA [18]. The high voltage

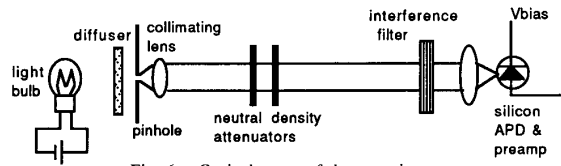


Fig. 6. Optical setup of the experiment.

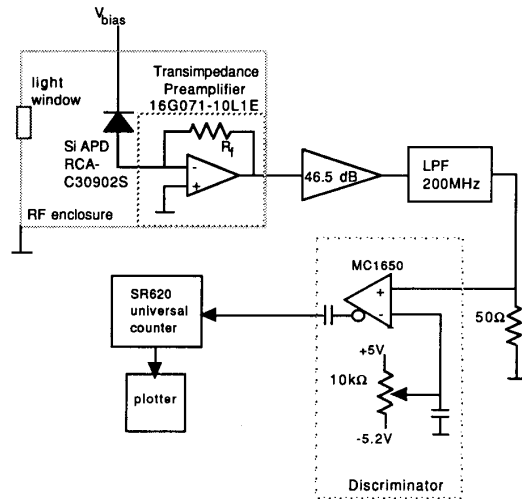


Fig. 7. Circuit diagram of the experimental nonbreakdown APD photon counter.

APD bias supply was generated by a dc-dc converter (Analog Modules, Model 521). The APD preamplifier consisted of a GigaBit Logic 16G071 transimpedance amplifier (dc-700 MHz, $R_f = 830\Omega$ [20]). The signal was further amplified to a level which was appropriate (~ 200 mV average peak pulse amplitude) for the discriminator. The lower cutoff frequency of the amplifier was about 100 KHz, which effectively filtered out $1/f$ noise from the preamplifier. A lowpass filter was used to block out the high frequency noise and the cutoff frequency (200 MHz) was chosen to correspond to the maximum speed of the discriminator. The gain-bandwidth product of the APD was greater than 300 GHz at an average APD gain of $G = 1000$ [2], which was sufficient for the experiment. The discriminator consisted of a high-speed comparator (Motorola MC1650).

B. Circuit Thermal Noise

The total circuit noise at the input of the comparator was measured with a RF power meter while biasing the APD about 100 V below its breakdown point so that the APD gain was essentially zero and its noise could be neglected. The total RF noise power measured was $2.5 \mu\text{W}$ over a bandwidth of 0.1–100 MHz. The net gain from the output of the preamplifier to the input of the discriminator was measured to be 46.5 ± 0.5 dB from 0.1 to 200 MHz with the -3 dB point at 220 MHz. The resultant equivalent noise current at the front end of the transimpedance amplifier was $6.4 \text{ pA}/\sqrt{\text{Hz}}$ (0.1–100 MHz), which was very close to that given by the data sheet ($5.7\text{--}6.3 \text{ pA}/\sqrt{\text{Hz}}$) [19]. The noise intensity rose by a few decibels over the frequency range of 100–200 MHz which

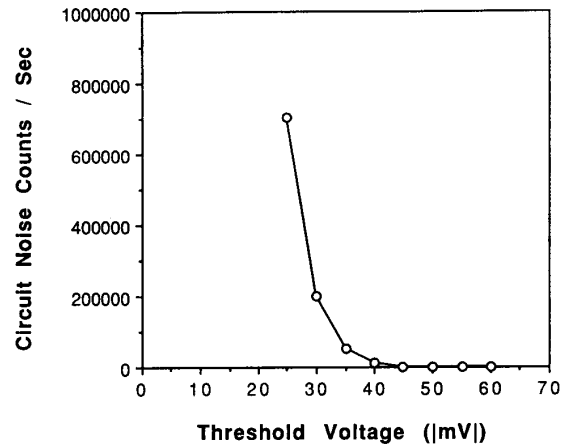


Fig. 8. Circuit thermal noise counts per second versus the absolute value of the threshold voltage applied at the comparator.

was believed to be caused by the packaging of the APD and the preamplifier. The total noise power measured at the input of the comparator was about $7.0 \mu\text{W}$ over the entire bandwidth. The corresponding equivalent noise current at the input of the APD preamplifier was $\sigma_{amp} = 0.107 \mu\text{A}$.

C. Measurements of Dark Counts and Photon Counts

The average noise counts due to the circuit thermal noise were first measured as a function of the absolute value of the threshold level applied at the comparator. The result is shown in Fig. 8. The APD was biased well below its breakdown point so that the contribution from the APD noise could be neglected. The counting interval was set to one second in this measurement and each point in Fig. 8 was based on the average of 100 measurements (sample size). The threshold voltage was measured at the negative input terminal of the comparator with the use of a digital multimeter. It is noticed that the effective threshold levels were higher than those measured at the comparator since the comparator had only limited gain and pulses at the positive input terminal had to exceed the threshold by a certain amount in order to trigger the subsequent counter.

The APD bias voltage was then increased to as close to the breakdown voltage (~ 252 V) as possible without an avalanche breakdown occurring at any time. An oscilloscope was used to monitor the APD preamplifier output to detect any possible avalanche breakdowns which appeared as abnormally large spikes in the output waveform. The actual average APD gain could not be measured directly because the APD was under CW illumination and the amplifiers were ac coupled. However, we had measured the average gain of another APD of the same model number under pulsed illumination and the highest average gain achieved was found to be 1000–1300.

The received optical power was adjusted to 1.0 pW . Fig. 9 shows the average waveforms of input pulses (negative going) and output pulses (positive going) of the comparator. It is noticed that the measured average pulse width (5.9 ns) was only approximate since it depended on the triggering level of the oscilloscope. The numbers of total counts and dark

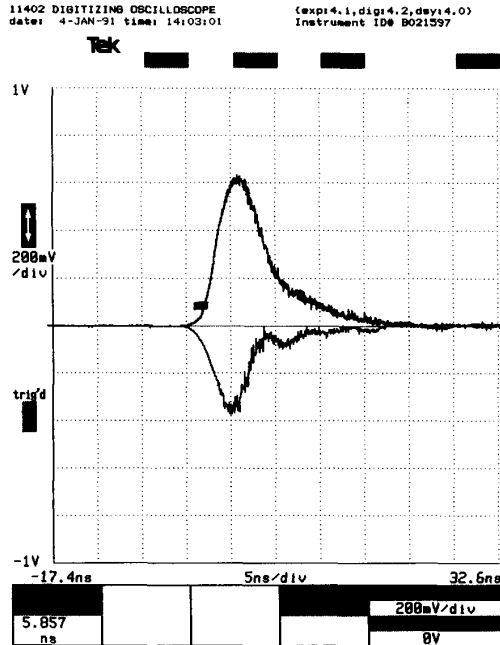


Fig. 9. Average waveforms of input pulses (negative going) and output pulses (positive going) of the comparator.

counts were measured as a function of the absolute value of the threshold voltage. The means and the standard deviations (error bar) of the measured counts are plotted in Fig. 10. The dark counts were measured while blocking the incident light beam. The counting interval was set to 1.0 millisecond and the sample size was 10^4 . Fig. 10 also shows the means and standard deviations of the thermal noise counts measured over the same counting interval for the same sample size (dot-dashed curve). The number of photon counts increased relatively slowly with the threshold level as compared to the total dark counts which included the circuit thermal noise counts. At low threshold levels, the circuit thermal noise counts became overwhelming and the standard deviations became abnormally large, as shown in Fig. 10. The optimal threshold should be at the "knee" of the dark counts curve.

Figs. 11–13 show the histograms of the thermal noise counts, the total dark counts, and the total counts under 1.0 pW received optical power when the threshold level was set to 47.1 mV. The counting interval was set to 1 ms and the sample size was 5×10^4 . The data shown on Figs. 11–13 are subject to the quantization error of the counter used which only output integers. Theoretically, the numbers of counts should all follow Poisson distributions and the ratio of the variance to the mean should be equal to unity. It was difficult to tell from Fig. 11 if the circuit thermal noise counts followed a Poisson distribution since there were too few counts in the 1 ms counting interval. The mean and the standard deviation measured over 1 s were about 900 and 100, respectively. Therefore the distribution of the circuit thermal noise counts was clearly not Poissonian in our experiment. This may be attributed to the fact that the circuit noise was somewhat

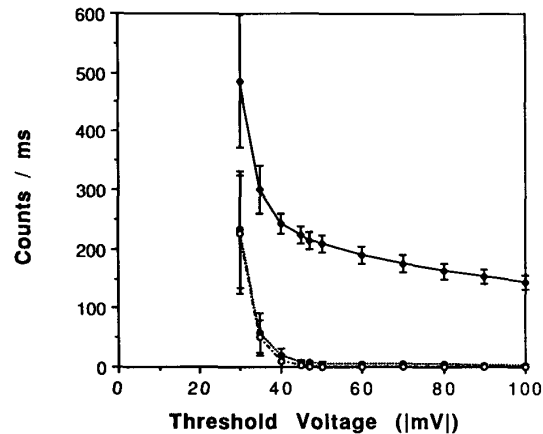


Fig. 10. Average number and standard deviation of the detected counts per millisecond under 1 pW received optical power as a function of the absolute value of the threshold voltage applied at the comparator (solid curve). The dot-dashed and the dotted curves represent the circuit thermal noise counts (when average APD gain $G = 0$) and the total dark counts (when $G \approx 1000$), respectively.

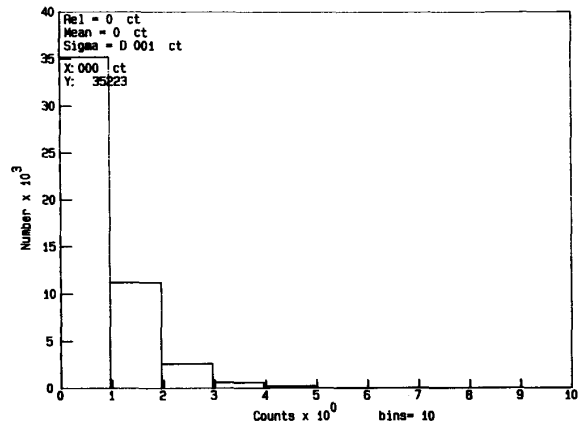


Fig. 11. Histogram of circuit thermal noise counts per millisecond. The sample size was 5×10^4 .

correlated and the noise power spectrum was not perfectly flat (white). The distributions of the total dark counts and total counts under 1.0 pW received optical power appeared to be Poissonian within the quantization error of the counter, as shown in Figs. 12 and 13.

D. Interarrival Times of the Photon Counts

The interarrival times of the observed counts were measured by splitting the comparator output into both Channels A and B inputs of the counter which measured the time interval started by a pulse at Channel A and stopped by the next pulse at Channel B. The input at Channel A was delayed by 4.66 ns through a coax cable to prevent the counter from being started and stopped by the same pulse. The two channels of the counter had to be well balanced so that the pulse sequence seen by Channel A was the same as that seen by Channel B.

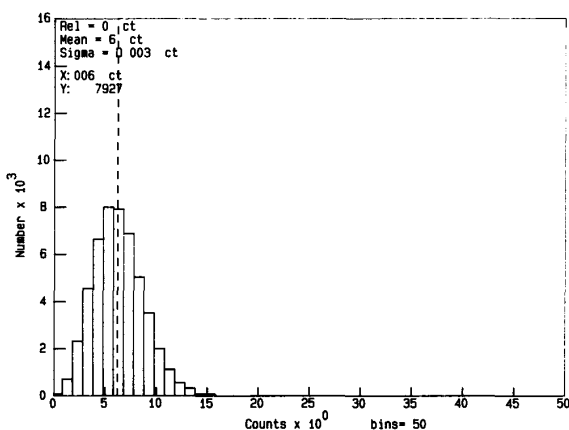


Fig. 12. Histogram of the number of the total measured dark counts per millisecond. The sample size was 5×10^4 .

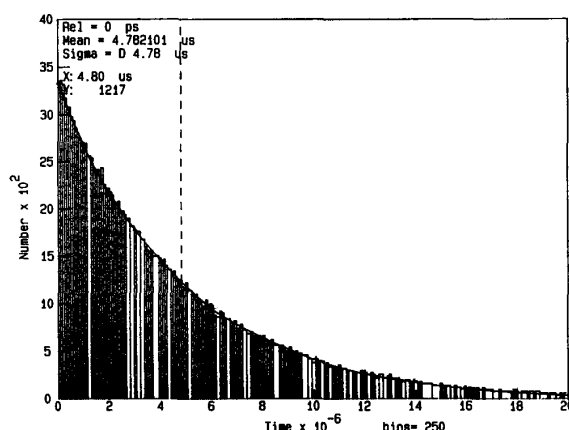


Fig. 14. Histogram of the interarrival times under 1 pW received optical power. The solid curve corresponds to the exponential distribution with the same mean (i.e., $3308 \times \exp[-t/4.78 \times 10^{-6}]$). The sample size was 2×10^5 .

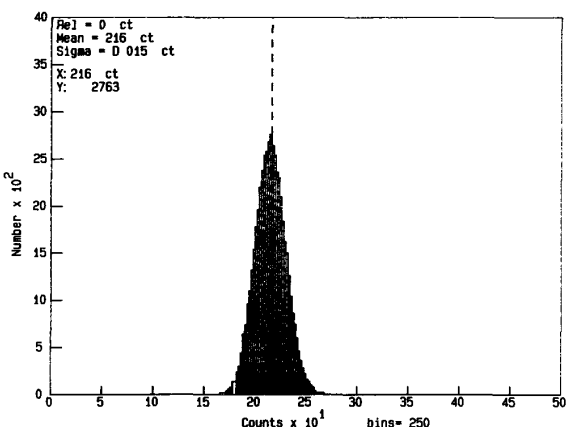


Fig. 13. Histogram of the number of the detected counts per millisecond under 1 pW received optical power. The sample size was 5×10^4 .

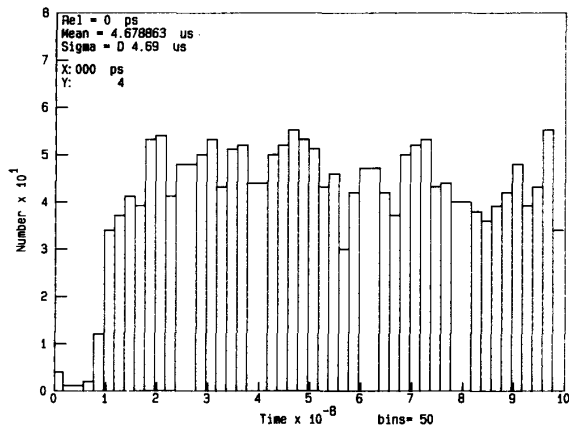


Fig. 15. Same as Fig. 14 but over an interarrival time range from 0 to 100 ns.

Fig. 14 shows a histogram of the measured interarrival time of the observed total number of counts under 1.0 pW received optical power. The sample size in this measurement was 2×10^5 . The heavy solid curve in Fig. 14 represents the theoretical values of the exponential distribution of the same mean. The measured interarrival times fit very closely to an exponential distribution which is an important property of a homogeneous Poisson random point process. Fig. 15 is a magnification of Fig. 14 from 0 to 100 ns. The sharp decrease near the origin was due to the dead time of the photon counter. The fluctuations in the histogram were due to the finite sample size of the measurements. The average dead time can be approximated as 15 ns after considering the coax cable delay (4.66 ns) at Channel A of the counter. As mentioned in the previous section, the dead time was a random number due to the randomness of the APD gain, the measured interarrival times could occasionally be shorter than the average dead time, as shown in Fig. 15.

E. Dynamic Range of the Photon Counter

Table I shows the mean and standard deviation of the total number of observed counts as a function of the received optical power. The fourth column shows the ratio of the variance to the mean of the measured counts (excluding the effect of the thermal noise counts). It is seen that the detected counts had a near Poissonian behavior up to 30 pW received optical power. The circuit seemed to start to saturate as the input optical power exceeded 30 pW. The threshold voltage was set to 47.1 mV so that the total number of dark counts was about $6 \sim 7$ /ms. Table I also lists the raw and the dead time corrected photon detection probabilities (excluding the dark counts). It is shown that the photon counter had a nearly constant photon detection probability of $P_{dcorr} \approx 5.0\%$ for up to 10 pW received optical power (2×10^6 cts/s). The dead time appeared to increase with the count rate due to the saturation of the electronics as the incident optical power exceeded 10 pW. The total number of counts versus the received optical power, the data in the first and second columns of Table I, are plotted in Fig. 16. The data measured at $\lambda = 1.064 \mu\text{m}$

TABLE I
MEASURED COUNTS VERSUS RECEIVED OPTICAL POWER.

P_o (pW)	cts/ms	σ	var/mean*	P_d^\dagger	P_{dcorr}^\ddagger
0.0	6	3	1.00	N/A	N/A
0.1	28	6	1.18	5.1%	5.1%
0.3	69	8	0.88	5.0%	5.0%
1.0	216	15	1.02	5.2%	5.2%
3.0	629	26	1.07	5.1%	5.1%
10	1990	43	0.93	4.8%	5.0%
30	5270	72	0.98	4.2%	4.6%
40	6510	87	1.16	3.9%	4.3%
50	7500	99	1.31	3.6%	4.1%
60	8670	107	1.32	3.5%	4.0%
70	9630	127	1.67	3.3%	3.9%
100	12.3×10^3	153	1.91	3.0%	3.6%
200	17.7×10^3	214	2.58	2.1%	2.9%
300	20.7×10^3	261	3.28	1.7%	2.4%
400	22.7×10^3	294	3.80	1.4%	2.1%
500	24.7×10^3	232	2.18	1.2%	1.9%

*var/mean = $(\sigma_{total}^2 - \sigma_{ther}^2) / (mean_{total} - mean_{ther})$ with the mean and the standard deviation of the circuit thermal noise counts, $mean_{ther} = 1$ and $\sigma_{ther} = 2$, respectively.

$\dagger P_d = (mean - mean_{dark}) / (P_o T / hf)$ with the counting interval, $T = 1$ ms, the received optical power, P_o , and the photon energy, $hf = 1.51$ eV ($\lambda = 820$ nm).

$\ddagger P_{dcorr} = P_d / [1 - (\tau_d / T) \bar{n}_c]$ with τ_d the dead time (15 ns) and \bar{n}_c the average number of detected counts.

are also plotted in Fig. 16. Those data were obtained by changing the interference optical filter in front of the APD. The statistical properties of the data at this longer wavelength were almost identical to those at $\lambda = 820$ nm. The curves in Fig. 16 tend to level off as the received optical power becomes extremely low because dark counts start to dominate. The curves also start to level off as the received optical power becomes relatively high because of the saturation of the circuit. The center segment of the curve is approximately linear and corresponds to photon detection probabilities of 5.0 and 0.33%, respectively. This closely agreed with the theoretically predicted value, 5.1 and 0.40% ($P_{disc} = 6.6\%$), according to (8)–(10) assuming that the average APD gain was $G = 1000$, APD quantum efficiency, $\eta_Q = 77\%$ at $\lambda = 820$ nm and $\eta_Q = 6.0\%$ at $\lambda = 1.064 \mu\text{m}$, the effective threshold current level, $I_{thr} = 4.5 \times \sigma_{amp}$ and $\sigma_{amp} = 0.107 \mu\text{A}$.

V. CONCLUSIONS

We have demonstrated that an APD can be used to count photons while being biased below its breakdown point. The major advantages of this type of APD photon counter versus a conventional Geiger mode APD biased above the breakdown point are the significantly shorter dead times and the total elimination of afterpulsing. A theoretical model has been

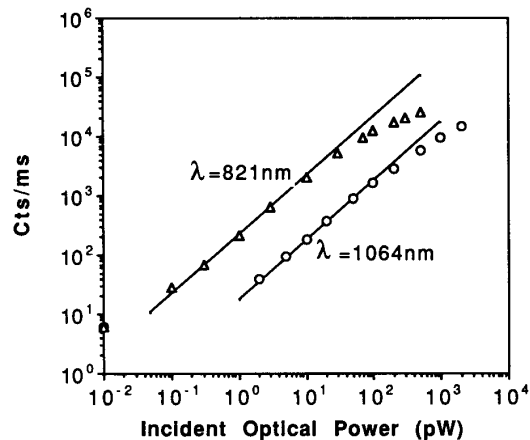


Fig. 16. Average number of detected counts per ms of the experimental nonbreakdown APD photon counter versus received optical power in pW.

developed to fully characterize this type of nonbreakdown APD photon counter. The theoretically predicted performance agreed well with the experimental measurements. The experimental nonbreakdown APD photon counter achieved a photon detection probability of 5.0% at $\lambda = 820$ nm and 0.33% at $\lambda = 1.064 \mu\text{m}$ under a dark count rate of about 7000/s at room temperature. The counting statistics appeared to follow a Poisson distribution and the interarrival times fit very tightly to an exponential distribution. The measured dead time of the photon counter was about 15 ns before the photon counter started to saturate and there was no afterpulsing observed. The experimental nonbreakdown APD photon counter has been shown to give better performance than a typical conventional breakdown type of APD photon counter.

The performance of the experimental nonbreakdown photon counter may be further improved by using more advanced silicon APD's and electronic components. One example is to use a state-of-the-art silicon APD developed by EG&G Canada [20], which has an extremely low hole-to-electron ionization coefficient ratio ($k_{eff} \approx 0.005$) and a 90% quantum efficiency at $\lambda \sim 820$ nm. The gain-bandwidth product and dark currents should be about the same as or better than the one we used (RCA-C30902S). We propose to use the same transimpedance preamplifier as the one in EG&G C30998-350 APD preamplifier modules, which has a 3-dB bandwidth of 350 MHz and an equivalent input noise current lower than $2\text{pA}/\sqrt{\text{Hz}}$ [21]. The equivalent threshold current is assumed to be still 4.5 times the rms circuit noise current so that the resultant dark count rate is still about 7000/second. The probability that an absorbed photon is discriminated under the above conditions becomes $P_{disc} = 22\%$. The predicted photon detection probability will be 20% at $\lambda = 820$ nm and 1.5% at $\lambda = 1.064 \mu\text{m}$ ($\eta_Q = 7\%$) with a dead time of a few nanoseconds. The linear dynamic range of the photon counter should also improve because of the wider electrical bandwidth. The performance of such a photon counter would be comparable to PMT's at $\lambda \sim 800$ nm and outperform PMT's at $\lambda = 1.064 \mu\text{m}$.

REFERENCES

- [1] Photomultiplier Tubes, Hamamatsu Corporation, Catalog, 1989, p. 77.
- [2] "High speed solid state detectors for fiber optic and very low light-level applications," RCA Inc., Electro Optics, Silicon avalanche photodiodes C30902E, C30902S, C30921E, C30921S (data sheet), 1988.
- [3] "Photodiode C30954E, C30955E, C30956 (data sheet)," EG&G Canada LTD., Optoelectronics Division, Jan. 1991.
- [4] T. E. Ingerson, R. J. Kearney, and R. L. Coulter, "Photon counting with photodiodes," *Appl. Opt.*, vol. 22, no. 13, pp. 2013-2018, July 1983.
- [5] K. Kikuchi, T. Okoshi, and A. Hirose, "Achievement of shot-noise-limited sensitivity and 50 dB dynamic range by photon-counting receiver using Si avalanche photodiode," *Electron. Lett.*, vol. 21, no. 18, pp. 801-802, Aug. 1985.
- [6] A. W. Lightstone and R. J. McIntyre, "Photon counting silicon avalanche photodiodes for photon correlation spectroscopy," in *Proc. OSA Top. Meet. Photon Correlation Tech. Applications*, May 31-June 2, 1988 (Washington, DC), pp. 183-191.
- [7] H. H. Tan, "Avalanche photodiode statistics in triggered-avalanche detection mode," TDA Progress Report 42-79 (N85-13 987), pp. 69-80, July-Sept. 1984.
- [8] P. G. W. Brown, K. D. Ridley, and J. G. Rarity, "Characterization of silicon avalanche photodiodes for photon correlation measurements. 1: Passive quenching," *Appl. Opt.*, vol. 25, no. 22, pp. 4122-4126, Nov. 1986.
- [9] P. G. W. Brown, R. Jones, J. G. Rarity, and K. D. Ridley, "Characterization of silicon avalanche photodiodes for photon correlation measurements. 2: Active quenching," *Appl. Opt.*, vol. 26, no. 12, pp. 2383-2389, June 1987.
- [10] B. I. Cantor and M. C. Teich, "Dead-time-corrected photocounting distributions for laser radiation," *J. Opt. Society Amer.*, vol. 65, no. 7, pp. 786-791, July 1975.
- [11] D. L. Snyder, *Random Point Processes*. New York: Wiley & Sons, 1975, p. 252.
- [12] R. J. McIntyre, "The distribution of gains in uniformly multiplying avalanche photodiodes: Theory," *IEEE Trans. Electron. Dev.*, vol. ED-19, no. 6, pp. 703-713, June 1972.
- [13] J. Conradi, "The distribution of gains in uniformly multiplying avalanche photodiodes: Experimental," *IEEE Trans. Electron. Dev.*, vol. ED-19, no. 6, pp. 713-718, June 1972.
- [14] M. L. Skolnik, *Introduction to Radar Systems*. New York: McGraw-Hill, 1962, p. 31-32.
- [15] R. G. Smith and S. D. Personick, "Receiver design for optical fiber communication systems," in *Semiconductor Devices for Optical Communications* H. Kressel Ed. New York: Springer-Verlag, 1980, ch. 4.
- [16] P. Horowitz and W. Hill, *The Art of Electronics*. New York: Cambridge Univ. Press, 1980, ch. 5.
- [17] B. Saleh, *Photoelectron Statistics*. New York: Springer-Verlag, 1978, p. 306.
- [18] X. Sun, "Free-space direct-detection optical communication with semiconductor laser transmitters and avalanche photodiode photodetectors," Ph.D. thesis, The Johns Hopkins University (Baltimore, MD), 1989, pp. 58-59.
- [19] GigaBit Logic 1991 GaAs IC Data Book & Designer's Guide, GigaBit Logic Inc., Newbury Park, CA, Aug. 1990, p. 5-26.
- [20] A. D. MacGregor, B. Dion, C. Noldeke, and O. Duchmann, "39 photons/bit direct detection receiver at 810 nm, BER = 1×10^{-6} , 60 Mb/s QPPM," in *Free-Space Laser Communication Technologies III* David L. Begley and Bernard D. Seery, Eds., proc. SPIE 1417, 1991.
- [21] Test data sheet of the transimpedance preamplifier modules C30998-350, EG&G Canada, Optoelectronics Division, 22001 Dumberry, Vaudreuil, J7V8P7, Canada, June 1991.



Xiaoli Sun (S'88-M'90) was born in Beijing, China, on May 3, 1956. He received the B.E. degree from Taiyuan Institute of Technology, Taiyuan, China, in January 1982, and the M.S.E. and Ph.D. degrees in electrical engineering from The John Hopkins University, Baltimore, MD, in May 1985 and May 1989, respectively.

He is currently an Associate Research Scientist in the Department of Electrical and Computer Engineering, The John Hopkins University. His research areas of interest are free-space optical communication systems and space-borne lidars.

Dr. Sun is a member of SPIE and Sigma Xi.



Frederic M. Davidson (M'74-SM'77) was born in Glens Falls, NY, on February 11, 1941. He received the B.S. degree in engineering physics from Cornell University, Ithaca, NY, in 1964, and the Ph.D. degree in physics from the University of Rochester, Rochester, NY, in 1969.

From 1968 to 1970, he was an Assistant Professor of Electrical Engineering at the University of Houston, Houston, TX. He joined the faculty of The John Hopkins University, Baltimore, MD, in 1970, and is currently a professor of the Department of

Electrical and Computer Engineering. His research areas of interest are optical communications and quantum electronics.

Dr. Davidson is a member of the Optical Society of America, SPIE, and Tau Beta Pi. He has also served as Associate Editor for Optical Communications for the IEEE Transactions on Communications from 1976 to 1986.